

# Structural Numerical Modelling Applied to the Capillary Barrier Effect Overburden of Acidic Tailings Ponds

Jianghong Du, QiuLing Xiong, Ailing Xun, Lu Zhang\*

Jilin University, Changchun, Jilin 130012, China

**Abstract:** *The issue of treating Acid Mine Drainage (AMD) has become a significant environmental concern for the global mining industry in recent years. AMD is generated by the leaching of sulfur-containing minerals (mainly pyrite, FeS<sub>2</sub>) in mine tailings, which react with atmospheric oxygen to form highly acidic solutions. These solutions contain heavy metal ions and pose significant risks to water bodies, soil, and human health. Moreover, the presence of AMD has been demonstrated to contribute to severe ecological damage, including the impairment of aquatic life through the induction of hypoxia in fish and other organisms. In light of the considerable impact of AMD, the treatment of this phenomenon has become an indispensable component of mining operations. The present study concentrates on the numerical simulation of the Capillary Barrier Effect Cover (CCBE) system applied to acid mine tailings. The CCBE consists of three layers: a coarse-grained soil layer at the base, a fine-grained soil layer in the middle, and a topsoil layer to prevent evaporation. The present study aims to analyse the influence of different structural configurations and material properties on the oxygen barrier performance of the CCBE, with particular focus on the effect of layer thickness on the system's efficiency in maintaining high saturation levels and preventing oxygen ingress into the tailings.*

**Key words:** Acid mine drainage, Numerical simulation, Capillary barrier effect cover, Column test.

## 1. Introduction

The management of Acid Mine Drainage (AMD) has emerged as one of the primary environmental challenges in the mining industry in recent years. AMD is formed during the leaching of sulfur-bearing minerals (primarily pyrite, FeS<sub>2</sub>) in mine tailings, which, upon exposure to atmospheric oxygen, undergoes oxidation and produces acidic solutions (Chen et al., 2021). These solutions contain high concentrations of heavy metals, leading to severe contamination of water bodies and soil, and presenting significant health risks to humans and wildlife. Furthermore, the presence of AMD has been shown to have extensive ecological consequences, typically manifesting as a yellow-brown liquid. This substance has been observed to impede water clarity and, moreover, to exert a deleterious effect on the viability of aquatic life, giving rise to a condition of oxygen deficiency (hypoxia) in fish and other organisms. The remediation of AMD is a multifaceted and protracted process, encompassing a range of methodologies for pollution control. A particularly efficacious approach involves the implementation of Capillary Barrier Effect (CCBE) cover systems, which are composed of multiple layers of soil exhibiting differing hydraulic properties. The bottom layer, composed of coarse-grained material, functions as an impermeable barrier to water, while the middle layer, composed of fine-grained material, serves as a water-retaining layer that maintains high moisture content and inhibits oxygen diffusion. The top layer, composed of coarse-grained soil, is designed to prevent evaporation and lateral water drainage.

The CCBE comprises three primary layers. The lowermost layer is the capillary break layers (CBL), which is composed of coarse-grained soil material and serves as a support. The middle layer is the moisture retaining layer (MRL), which consists of fine-grained soil material with a saturation level of 85 per cent or more (Kalonji Kabambi et al., 2017). This layer is characterised by a low hydraulic conductivity, which effectively restricts oxygen diffusion and transportation. The

MRL can act as a barrier to oxygen because oxygen diffuses and transports very slowly in water. At the top of the cover is the topsoil layer, which consists of coarse-grained soil material used to limit water evaporation and lateral drainage. A capillary barrier is formed between the fine-grained and coarse-grained layers due to the difference in unsaturated hydraulic conductivity, thereby limiting oxygen migration and water infiltration into the downward movement of the overburden and maintaining high saturation (Sr) of the fine-grained soil. The maintenance of high saturation in the water storage layer has been shown to significantly reduce the oxygen diffusion coefficient, thereby preventing oxygen from entering the acidic tailings. The investigation by Nicholson et al. in 1989 revealed that the performance of the CCBE is predominantly influenced by the characteristics of the fine- and coarse-grained soils (Nicholson et al., 1989). Within a reasonable range, the greater the difference in soil particle size, the greater the differences in hydraulic conductivity characteristics, and the more effective the barrier effect in restricting water infiltration. This is conducive to the increase of saturation in the fine-grained soils with poor permeability. A seminal study by Ross et al. in 1990 provided a comprehensive investigation into the hydraulic conductivity of the coarse-grained layer at the base of the mulch layer, along with the associated calculation method (Ross, 1990). In 1995, Aubertin et al. systematically defined the layers of CCBE and investigated the effective size range (Aubertin 1995). Subsequently, in 2023, Gao Cen et al. investigated the quantitative calculation of the capillary barrier effect at various important time points, such as the time of arriving at each layer, the time of the capillary barrier effect being overcome, etc. (Gao et al., 2023). Bussière found that, regarding the structure of CCBE, there are two main types applied to acidic tailings pond management: fine-coarse and coarse-fine-coarse (Bussière, 1999). Whereas the fine-coarse-fine pairing is mainly applied to landfills (Abichou et al., 2009) and to the containment of slopes. The rationale behind this discrepancy lies in the divergent management objectives of

the two sites. The fine-coarse-fine structure applied to landfills places greater emphasis on seepage control performance, whereas the oxygen and acid barrier performance of the cover layer is paramount in the context of acidic tailings ponds. Coarse-fine-coarse structure is frequently employed in the case of acidic tailings ponds, and the four- or even five-layered structure is often utilised in the context of vegetation cover to ensure the stable growth of the overlying vegetation rhizome and the stability of the vegetation cover. Drawing upon these analyses conducted by researchers, this paper will systematically investigate the effects of the structure and dimensional parameters of CCBE on its oxygen barrier properties.

## 2. Methods and Materials

### 2.1 Materials and Characterization

#### 2.1.1 Material Properties

In this study, the CCBE system is investigated through a combination of laboratory column experiments and numerical simulations. The coarse-grained soil employed in the experiments consists of sand, while the fine-grained soil is silt. The particle size distributions for these soils were measured using a laser diffraction particle size analyser (ASTM D422), and both constant head and falling head tests were performed to determine the saturated permeability. The results obtained are summarised as follows:

**Table 1:** Properties of Materials

Soil Type	Bulk Density ( $\rho_s$ )	Saturated Permeability (cm/s)
Coarse Sand	1.56 g/cm <sup>3</sup>	0.15
Silty Soil	1.53 g/cm <sup>3</sup>	0.0001

#### 2.1.2 Soil-Water Characteristic Curve

Soil-water characteristic curves are a representation of the hydraulic properties of soil, which have a significant impact on the performance of CCBE. The soil-water characteristic curve is primarily concerned with the volumetric water content-matric suction curve and the unsaturated hydraulic conductivity-matric suction curve. The method for obtaining these two curves is as follows: Firstly, experimental data for volumetric water content and matric suction are obtained. Subsequently, the parameters  $\alpha$  and  $n$  are estimated through the utilisation of the Van Genuchten equation model (van Genuchten, 1980). Finally, the unsaturated hydraulic conductivity-matric suction curve is estimated based on the relationships between  $\alpha$ ,  $n$ , saturated water content, residual water content, and the volumetric water content-matric suction curve. The significance of these two curves lies in their role in defining material properties when employed in numerical simulation software.

### 2.2 Column Design

This study constructed a hollow acrylic column for the column experiments, which was designed with a three-section

structure corresponding to the moisture retention layer, water-holding layer, and support layer of the CCBE. Each section of the column has a diameter of 30 cm, with heights designed according to standard specifications. From bottom to top, the heights of the three sections are 40 cm, 50 cm, and 50 cm, respectively. The uppermost section was elevated above the soil layer to enable the incorporation of water. To prevent water leakage between the sections, flange connections were employed, facilitating more efficient soil compaction. Pre-drilled holes for sensor placement were created on both sides of the column. The centres of these holes are located at distances of 10 cm, 30 cm, 50 cm, 65 cm, 80 cm, 100 cm, 115 cm and 130 cm from the bottom of the column, thus resulting in a total of 16 holes. Additionally, a drain with a switchable valve is installed at the bottom. Prior to the commencement of the experiment, the valve is closed to enable the saturation of the soil within the column. During the experiment, the valve is opened to simulate the drainage of water from the bottom, thereby replicating real field conditions. During the soil filling process, sensors are inserted through the holes into the soil to obtain real-time data with minimal disturbance to the soil structure. The volumetric water content sensors employed were of the Decagon Devices EC-5 model, whilst the water potential sensors utilised were of the METER Environment Teros-21 model, ranging from -9 kPa to -100,000 kPa. Both types of sensors are operational within a temperature range of -40°C to 60°C, which meets the requirements of the present study. Furthermore, a 10 cm high rainfall simulator was designed above the soil column. The base area of the simulator matches the bottom area of the column, with 30 pinholes evenly distributed to ensure uniform rainfall. A Mariotte bottle with a diameter of 25 centimetres, of cylindrical form, is affixed above the simulator in order to ensure a stable water supply rate. The rainfall rate is set to match the maximum daily rainfall intensity of 35 millimetres per hour for the study area.

### 2.3 Numerical Simulation Analysis

In section 2.1.2, the soil-water characteristic curves measured in the experiment are entered, specifically the volumetric water content function and permeability function. To obtain the volumetric water content function, the parameters  $\alpha$ ,  $n$ , saturated volumetric water content, and residual volumetric water content are input, which will generate the function graph. The unsaturated permeability coefficient graph is obtained by employing the software's integrated functionality and the Van Genuchten method, in conjunction with the saturated permeability coefficient. The selection of boundary conditions is informed by the prevailing local climate conditions, as illustrated in Figure 1. Within the study area, precipitation is observed to be most concentrated from July to September, aligning with the rainy and hot season. The maximum precipitation in 2022 occurred in July, with a total monthly precipitation of 179.6 mm, and the maximum daily precipitation was 35 mm. The average monthly temperature was 22.9°C, which represents the typical climate conditions of Northeast China. The numerical simulation analysis in this study was conducted based on this climate as the boundary condition.

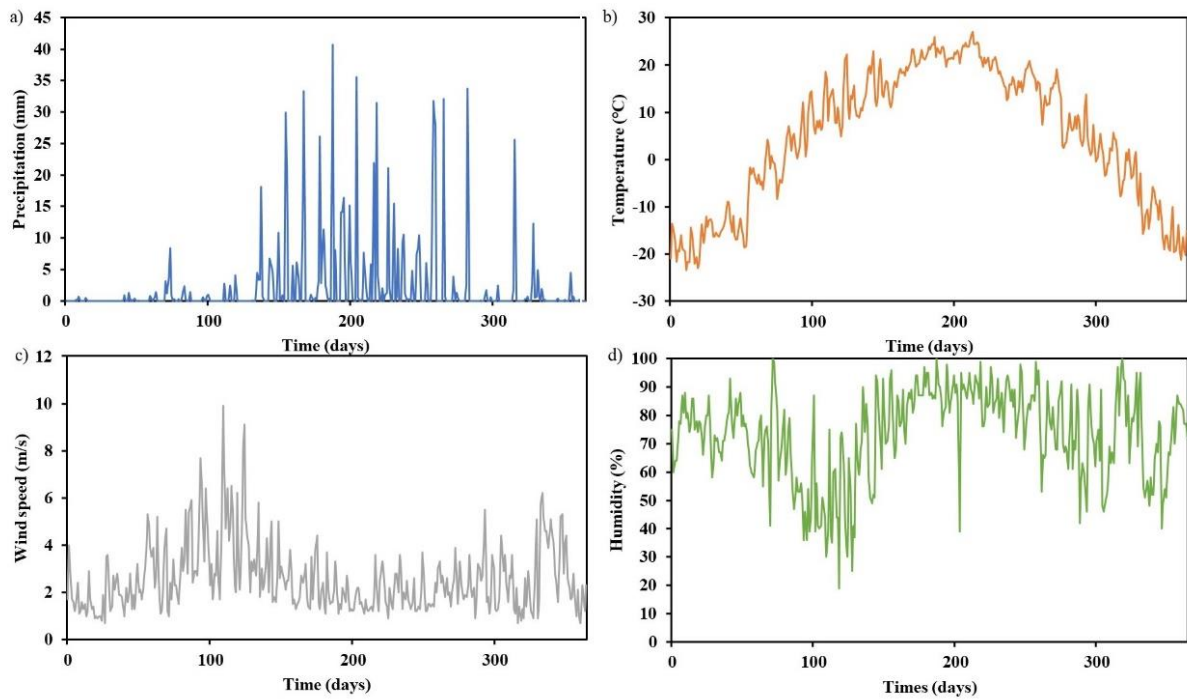


**Figure 1:** Weather conditions: a) Precipitation; b) Temperature; c) Wind speed; d) Humidity

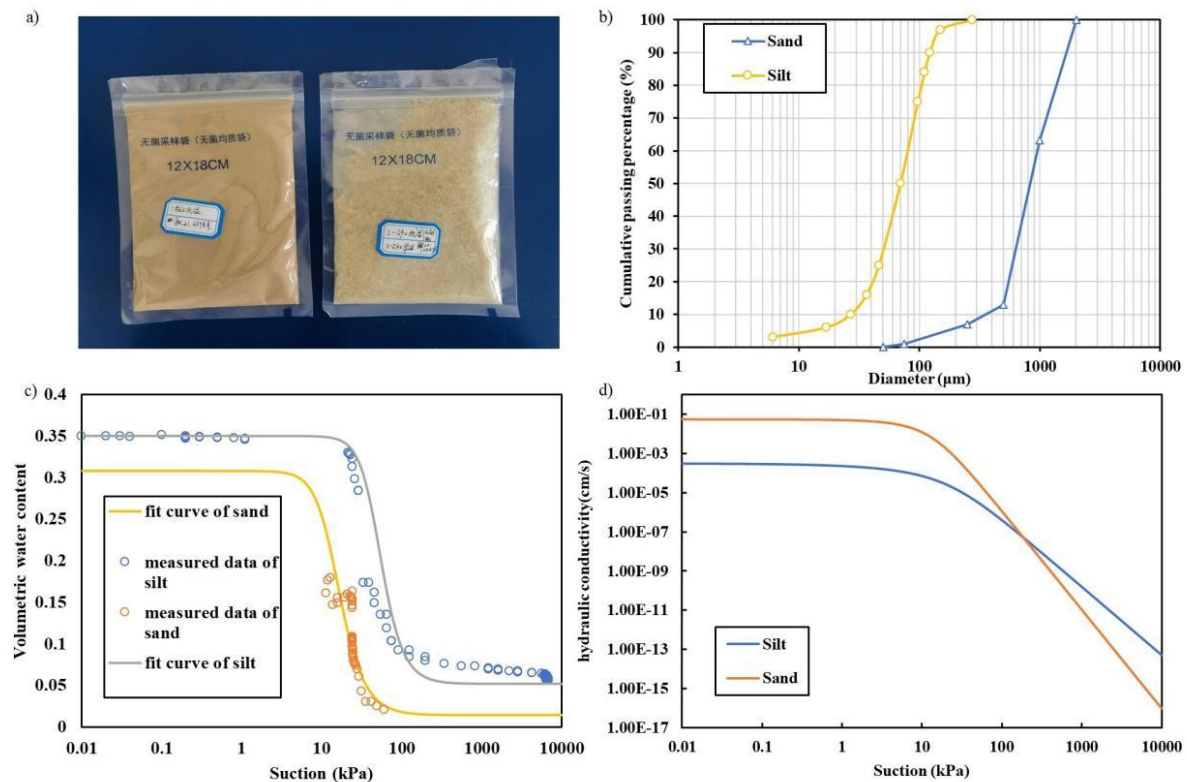


**Figure 2:** a) Soil samples for column experiments; b) Grain-size distribution of the sand and silt; c) Typical water retention curve measured in the laboratory for the testing materials; d) Permeability functions measured in the laboratory for the testing materials

### 3. Results and Discussion

#### 3.1 Material Characterization

As demonstrated in Figure 2(b), the particle size distribution of the silty soil and sandy soil utilised in the column experiments reveals that the majority of particles in the silty soil have diameters concentrated in the range of 0.01-0.1 mm,

while the majority of particles in the sandy soil fall within the particle size range of 0.5-1 mm. The experimental data for their matric suction, as depicted in Figure (c), were fitted using the Van Genuchten model to obtain their Soil-Water Characteristic Curves (SWCCs), by correlating their entry values and  $n$  parameters. The specific parameter values are shown in Table 2.

**Table 2:** Basic and hydraulic properties of materials used in experimental columns and numerical modelling

Parameters	Sand	Silt
Air entry value (kPa)	8	48
$\theta_r$	0.014	0.052
$\theta_s$	0.3077	0.35
n	3.2	3.56
ps	1.56	1.53

### 3.2 Fitting of Column Experiments to Numerical Simulations

As demonstrated in Figure 3, a comparison is made between the volumetric water content within the soil from the column experiment and the simulation results of SEEP/W. It is evident that the simulation results align closely with the measured data, with the former being marginally larger than the latter. Furthermore, the trend exhibited by the data is nearly identical. In both cases, the saturation levels of the top protective layer and the bottom water-insulating layer decreased rapidly to very small values within the 24-hour time period, while the water-retaining layer in the middle was consistently in a state of high saturation. Some acceptable deviations of the actual data points from the numerical simulation results were found in the fitting of the two, which can be attributed to the fact that only SEEP/W was used in this simulation for the numerical simulation of the seepage field without considering the effects of other physical fields. For example, the effect of the thermodynamic field on the evaporation was not taken into account, and the evaporation was only estimated using Penman-Monteith. Additionally, the absence of radiation data in this numerical simulation led to the utilisation of local outdoor radiation data from the laboratory, which resulted in an overestimation of evaporation due to the significantly higher solar radiation energy levels in comparison to the actual indoor conditions. The relative accuracy of this numerical simulation is evidenced by the preservation of the overall trend and the absence of significant data deviation. The successful calibration of this model provides a foundation for subsequent, more extensive numerical simulation studies that will be based on this model.

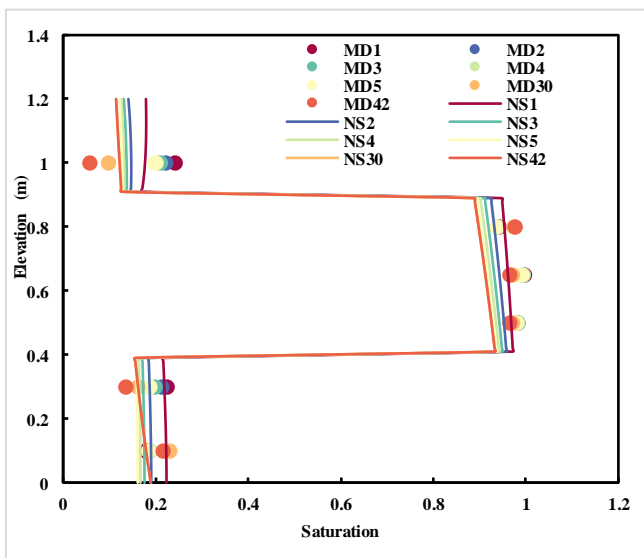


**Figure 3:** Fitting of measured data to numerical simulation analysis results

### 3.3 Influence of CCBE Structure

According to Bussière et al. (1999), two main types of capillary barrier cover applied to acidic tailings cover are distinguished: fine-coarse and fine-coarse-fine. In this section, in addition to these two types, a non-capillary barrier cover pure fine-grained soil model is included for comparison to observe the effects imposed by the capillary barrier cover. The material soils were selected to be natural soils, i.e. natural coarse sand and silt from column 3.2 experiments and numerical simulations in 4.2. The boundary conditions were chosen to be the climatic conditions of the study area throughout the year 2022. The simulation results are shown in Figures 4 and 4. The study point location chosen for this data curve is the location of sensor #2, which is the upper part of the water retention layer. The rationale behind selecting this particular point is twofold: firstly, the evaporation protection provided by the layer can be more readily observed, and secondly, this sensor point is the closest to the top, thus making it relatively more sensitive to evaporation. As illustrated in Figure 4, the volumetric water content of the pure fine-grained soil cover is consistently lower compared to the remaining two capillary barrier covers throughout the year. It is particularly evident during periods of heavy summer rainfall that the volumetric water content exhibits significant variations, demonstrating a high sensitivity to precipitation, reaching a low value of approximately 0.2 during seasons with limited rainfall, which does not result in the isolation of oxygen. This observation underscores the efficacy of the capillary barrier cover.

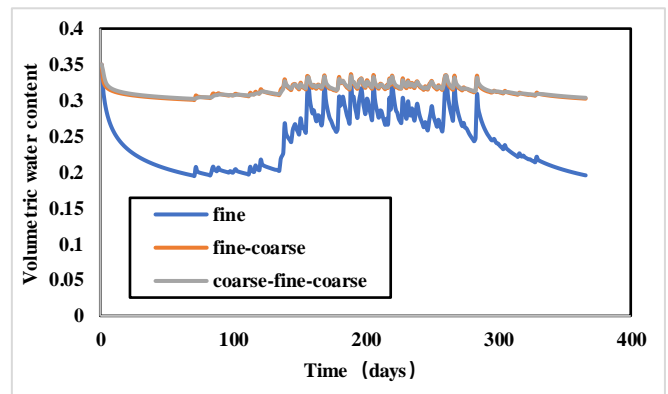


**Figure 4:** Year-round variation in volumetric water content of the fine-grained layer in the three cover layers

The volumetric water content of the two types of capillary barrier cover is illustrated in Figure 5. Due to the considerable interval between the axes, the data for both types are analysed separately. This is achieved by reducing the range of the axes to facilitate detailed observation, as demonstrated in Figure 5. It is evident that during the low rainfall seasons of 0-70 days and 330-365 days, the three-layer capillary barrier cover is significantly less affected by evaporation than the two-layer capillary barrier cover due to its protective layer and exhibits a more stable performance in the face of drought conditions. In the presence of rainfall, it is evident that the saturation levels of the three-layer capillary barrier cover are less pronounced compared to those of the two-layer cover, due to the necessity of replenishing the protective layer from above. However, the difference in values is not statistically significant. Consequently, it can be deduced that in regions with four distinct seasons, characterised by abundant precipitation and relatively infrequent drought periods, the implementation of a double-layer capillary barrier cover is

more efficacious. Conversely, in regions with four seasons, such as the Northeast, the employment of a triple-layer capillary barrier cover is more effective in preventing the reduction of saturation induced by prolonged droughts, i.e. the decay of the oxygen barrier performance.

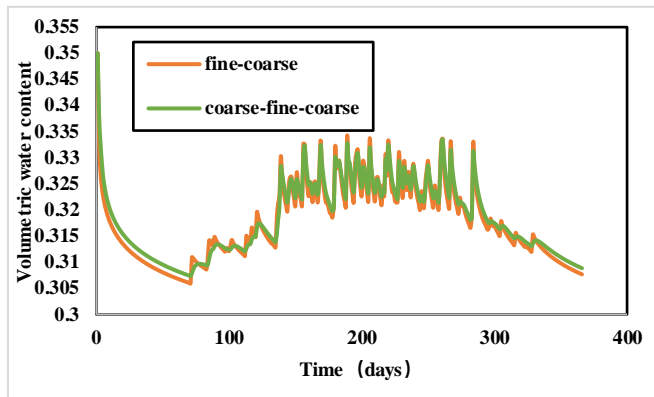


**Figure 5:** Year-round variation in MRL volumetric water content for both CCBEs

### 3.4 Influence of the Thickness of the Layers of CCBE

Bussi re's theory posits that, in order to form an effective capillary barrier cover in a coarse-fine-coarse structure, the thickness of the coarse-grained soil layer must exceed 0.3 m, while the fine-grained soil layer must have a minimum thickness of 0.5 m. This section is thus based on the thicknesses of the layers in 3.2, with the understanding that thicknesses of two of the layers and only changing the remaining layer, TOP CBL and BOTTOM CBL respectively, starting from 0.3m and increasing in 0.1m increments until it increases to 1.5m. MRL, on the other hand, starts from 0.5m and increases in 0.1m increments until it reaches 1.5m. This

approach enabled the formulation of numerous comparative numerical simulation analyses, which were then utilised to analyse the patterns based on the results and to explore the effect of each layer thickness on the final saturation level. This process was undertaken with the objective of providing more accurate suggestions for the site construction. Initially, the influence of the thickness of the support layer on the overall performance of the capillary barrier cover layer was investigated. The results of each numerical simulation were summarised as shown in Figure 6. Figure 6a records the change in saturation of the capillary barrier overlay throughout the year for different thicknesses of the water barrier layer. The point selected is the location of sensor No. 2 because this point is the most sensitive to changes in the weather. The effect of the change in evaporation brought about by changes in the thickness of the protective layer can be most efficiently observed in relation to the difference in the saturation of the water retention layer. Figure 6b presents the annual variation in saturation at sensor location #4, as this point typically exhibits the highest saturation levels, thereby demonstrating the optimal performance of the capillary barrier overlay. Figure 6c illustrates the relationship between the lowest point value of saturation and the thickness of the protective layer. It is evident that an increase in the thickness of the support layer results in enhanced oxygen barrier performance of the capillary barrier covering layer. However, the actual change value is not particularly discernible. The boundary conditions explored in this numerical simulation do not encompass drought conditions, thereby obscuring the impact of thickness variations in the support layer on the overall oxygen barrier performance of the capillary barrier cover layer. Furthermore, the lowest saturation degree is observed on the same day irrespective of thickness variations in the support layer.

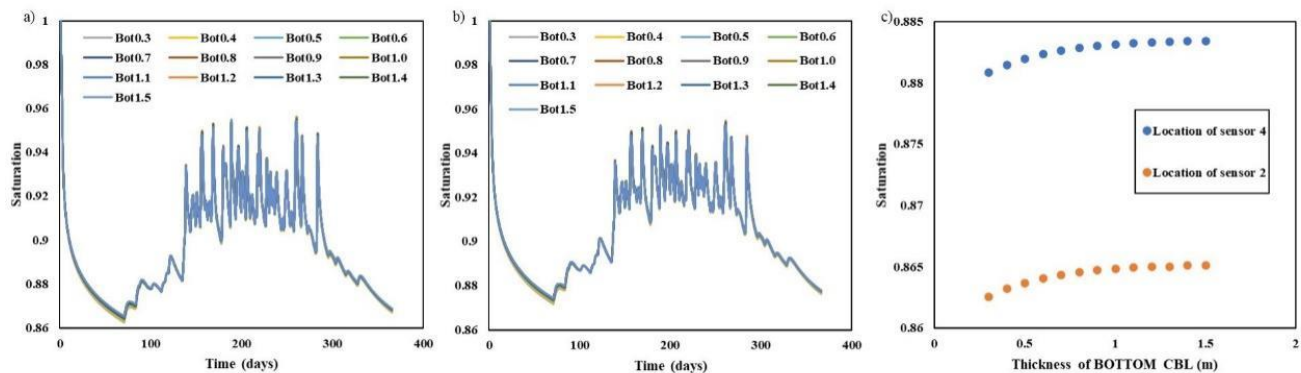


**Figure 6:** Variation of saturation at different locations of CCBE with different Bottom CBL thicknesses throughout the year  
a) Sensor 2 b) Sensor 4 c) Variation of minimum saturation with Bottom CBL thicknesses

Figures 7a and 7b illustrate the variations in saturation level throughout the year in the capillary barrier overlay for varying thicknesses of the water-retention layer for sensor numbers 2 and 4, respectively. The data variation at sensor position 2 clearly demonstrates that the difference in saturation level due to the thickness of the water retention layer is substantial, with the saturation level at this position exhibiting a slight decrease for every 0.1m increase in layer thickness. This phenomenon

can be attributed to the fact that a thicker water retention layer necessitates a greater volume of water to maintain a high level of saturation. Consequently, when designing the thickness of the water retention layer, two factors must be considered: firstly, the necessity to ascertain the thickness of the water retention layer in accordance with the specific conditions of the local area, and secondly, the consideration of the increased economic cost of the additional material required.

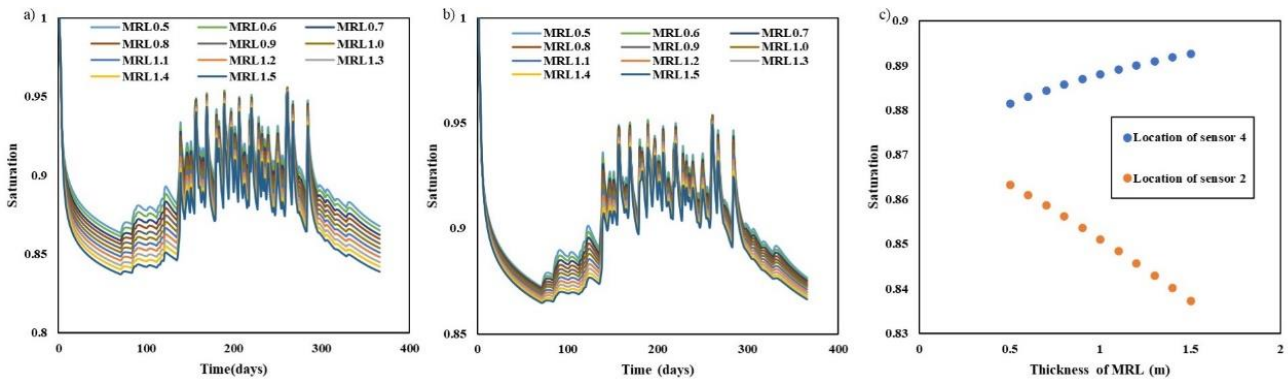


**Figure 7:** Variation of saturation at different locations of CCBE with different MRL thicknesses throughout the year a) Sensor 2 b) Sensor 4 c) Variation of minimum saturation with MRL thicknesses

As demonstrated in Figure 8, the numerical simulation results for the thickness variation of Top CBL reveal a trend of saturation with the thickness of the protective layer at the positions of sensors No. 2 and No. 4. This trend is situated between the trend of saturation with the variation of Bottom CBL and MRL. The saturation of both positions exhibits an increasing trend with the thickness of the protective layer, which is advantageous to the oxygen barrier performance of CCBE. It is noteworthy that with an increase in the thickness of the protective layer, the time of the lowest saturation is postponed, and the lowest saturation exhibits an upward trend. The thickness of Top CBL directly correlates with its

resistance to evaporation, thereby influencing the replenishment of water to the MRL. Evaporation, being a detrimental factor, exerts a significant adverse effect on the capillary barrier cover in the Northeast. In order to adapt construction to local conditions, greater attention must be paid to the design of the protective layer when installing a capillary barrier cover in the Northeast, particularly in locations where there is a lack of vegetation in the vicinity and where the albedo is too low. The benefits of increasing the thickness of the protective layer are the most obvious and straightforward to achieve, and do not require an excessive increase in cost to bring about a higher increase in oxygen barrier performance.

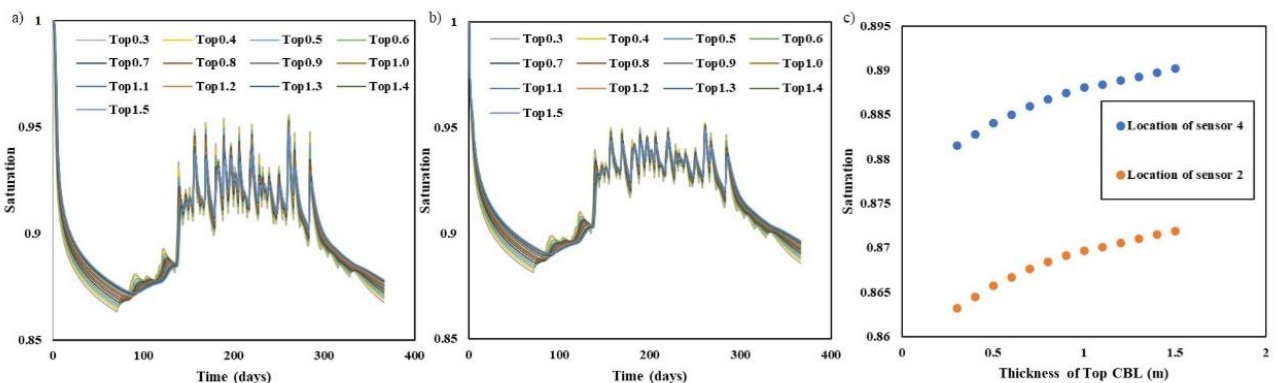


**Figure 8:** Variation of saturation at different locations of CCBE with different Top CBL thicknesses throughout the year a) Sensor 2 b) Sensor 4 c) Variation of minimum saturation with Top CBL thicknesses

#### 4. Conclusion

This research unequivocally demonstrates that the Capillary Barrier Effect represents a highly efficacious strategy for the management of acid mine tailings. Among the various configurations investigated, the coarse-fine-coarse structure has emerged as the preeminent choice, exhibiting remarkable proficiency in upholding elevated water saturation levels within the system and effectively thwarting the ingress of oxygen. The outcomes of this study underscore the critical significance of meticulously optimizing the thicknesses of the individual layers of the CCBE in accordance with the specific climatic idiosyncrasies of the site in question. By doing so, the CCBE system can be engineered to perform optimally throughout both arid and humid seasons, ensuring robust and consistent functionality. Future research endeavors should be resolutely directed towards the refinement of the numerical model employed herein, with the ultimate aim of enhancing its precision and predictive capabilities. Additionally, efforts

should be made to extrapolate and apply the findings of this study to large-scale, real-world applications in the domain of acid mine drainage treatment, thereby facilitating more sustainable and environmentally sound mining practices on a broader scale.

#### Acknowledgments

This work was supported by Graduate Innovation Fund of Jilin University.

#### References

[1] Abichou, T., Mahieu, K., Yuan, L., Chanton, J., & Hater, G. (2009). Effects of compost biocovers on gas flow and methane oxidation in a landfill cover. *Waste Management*, 29(5), 1595–1601. <https://doi.org/10.1016/j.wasman.2008.11.007>

- [2] Bussière, B. (1999). *Étude du comportement hydrique de couvertures avec effets de barrières capillaires inclinées à l'aide de modélisations physiques et numériques* [Phd, École Polytechnique de Montréal]. <https://publications.polymtl.ca/8726/>
- [3] Chen, G., Ye, Y., Yao, N., Hu, N., Zhang, J., & Huang, Y. (2021). A critical review of prevention, treatment, reuse, and resource recovery from acid mine drainage. *Journal of Cleaner Production*, 329, 129666. <https://doi.org/10.1016/j.jclepro.2021.129666>
- [4] Gao, C., Ye, W.-M., Lu, P.-H., Liu, Z.-R., Wang, Q., & Chen, Y.-G. (2023). An infiltration model for inclined covers with consideration of capillary barrier effect. *Engineering Geology*, 326, 107318. <https://doi.org/10.1016/j.enggeo.2023.107318>
- [5] Kalonji Kabambi, A., Bussière, B., & Demers, I. (2017). Hydrogeological Behaviour of Covers with Capillary Barrier Effects Made of Mining Materials. *Geotechnical and Geological Engineering*, 35(3), 1199–1220. <https://doi.org/10.1007/s10706-017-0174-3>
- [6] Nicholson, R. V., Gillham, R. W., Cherry, J. A., & Reardon, E. J. (1989). Reduction of acid generation in mine tailings through the use of moisture-retaining cover layers as oxygen barriers. *Canadian Geotechnical Journal*, 26(1), 1–8. <https://doi.org/10.1139/t89-001>
- [7] Ross, B. (1990). The diversion capacity of capillary barriers. *Water Resources Research*, 26(10), 2625–2629. <https://doi.org/10.1029/WR026i010p02625>
- [8] van Genuchten, M. Th. (1980). A Closed-form Equation for Predicting the Hydraulic Conductivity of Unsaturated Soils. *Soil Science Society of America Journal*, 44(5), 892–898. <https://doi.org/10.2136/sssaj1980.03615995004400050002x>